DALTON
FULL PAPER

Contemporary bimetallic molecules: an unusual class of *exo-closo* metallacarbaboranes having no metal–metal bonds

Dianne D. Ellis, Andreas Franken, Paul A. Jelliss, Jason A. Kautz, F. Gordon A. Stone* and Pui-Yin Yu

Department of Chemistry and Biochemistry, Baylor University, Waco, TX 76798-7348, USA

Received 11th May 2000, Accepted 13th June 2000
Published on the Web 17th July 2000

Reactions between cationic metal–ligand fragments and salts of the anionic complexes [2,2,2-$(CO)_3$-2-PPh_3-*closo*-2,1-$MoCB_{10}H_{11}$]$^-$ and [2,2-$(CO)_2$-2-L-*closo*-2,1-$FeCB_{10}H_{11}$]$^-$ (L = CO or PPh_3) have afforded a range of zwitterionic compounds in which an electrophilic $[ML'_n]^+$ group is attached to the cage system in an exopolyhedral manner by one, two, or three agostic B–H⟶ML'_n bonds. The bimetal compounds isolated do not have direct metal–metal bonds, a feature confirmed by X-ray diffraction for [2,2,2-$(CO)_3$-2-PPh_3-7,8,12-(μ-H)$_3$-7,8,12-{$Cu(PPh_3)$}-*closo*-2,1-$MoCB_{10}H_8$], [2,2,2-$(CO)_3$-2-PPh_3-7,12-(μ-H)$_2$-7,12-{$Ag(PPh_3)$}-*closo*-2,1-$MoCB_{10}H_9$], [2,2,2-$(CO)_3$-2-PPh_3-7,8,12-(μ-H)$_3$-7,8,12-{$RuCl(PPh_3)_2$}-*closo*-2,1-$MoCB_{10}H_8$] and [2,2,2-$(CO)_3$-2-PPh_3-12-(μ-H)-12-{$Fe(CO)_2(\eta\text{-}C_5Me_5)$}-*closo*-2,1-$MoCB_{10}H_{10}$]. The penultimate compound displays in solution complicated dynamic behaviour, in part due to the presence of a number of diastereomeric pairs of enantiomers. Low temperature $^{31}P\text{-}\{^1H\}$ NMR data have helped elucidate these processes for the isomers observed for this complex. The NMR data (^1H, ^{13}C, ^{11}B, and ^{31}P) for the new compounds are discussed.

Bimetallic metal complexes in which a [7,8-R_2-*nido*-7,8-$C_2B_9H_9]^{2-}$ (R = H or Me) ligand bridges a metal–metal bond have been known for several years.[1] In these species a metal atom M is pentahapto coordinated by the open CCBBB face of the cage forming a *closo*-3,1,2-MC_2B_9 framework. The exopolyhedral M–M′ bond is supported by one or two agostic B–H⟶M′ linkages, with the former situation more prevalent. These bonds may involve B–H groups in either the *α* (CC*B*BB) or the *β* (CCB*B*B) sites with respect to the carbon in the pentagonal C_2B_3 ring ligating the atom M. We have more recently developed a new class of molecule where the carbaborane bridges two metal centres with no metal–metal bond present.[2] Thus the anionic rhenacarbaborane carbonyl complex [3,3,3-$(CO)_3$-*closo*-3,1,2-$ReC_2B_9H_{11}$]$^-$ functions as a ligand by coordinating cationic metal ligand fragments. Treatment of its caesium salt Cs[3,3,3-$(CO)_3$-*closo*-3,1,2-$ReC_2B_9H_{11}$] **1** with [$RuCl_2(PPh_3)_3$], [$RhCl(PPh_3)_3$] or [$Fe(CO)_2$(THF)-(η-C_5H_5)][BF_4] affords, respectively, the zwitterionic compounds [3,3,3-$(CO)_3$-8,9,12-(μ-H)$_3$-8,9,12-{$RuCl(PPh_3)_2$}-*closo*-3,1,2-$ReC_2B_9H_8$] **2**, [3,3,3-$(CO)_3$-8,9-(μ-H)$_2$-8,9-{$Rh(PPh_3)_2$}-*closo*-3,1,2-$ReC_2B_9H_9$] **3**, and [3,3,3-$(CO)_3$-8-(μ-H)-8-{$Fe(CO)_2$-(η-C_5H_5)}-*closo*-3,1,2-$ReC_2B_9H_{10}$] **4**. In the bimetal species **2**–**4** the *closo*-3,1,2-$ReC_2B_9H_{11}$ cage donates six, four and two electrons, respectively, *via* the B–H⟶M (M = Ru, Rh or Fe) bonds to the exopolyhedrally bound metal centre.

We are concurrently developing the chemistry of monocarbon metallacarbaborane complexes, a class of compound that has been little studied up to the present time. Species prepared recently in our laboratory include $[N(PPh_3)_2]$[2,2,2-$(CO)_3$-*closo*-2,1-$ReCB_{10}H_{11}$] **5**,[3] [$N(PPh_3)_2$][2,2,2-$(CO)_3$-2-L-*closo*-2,1-$MoCB_{10}H_{11}$] **6a** (L = CO), **6b** (L = PPh_3) and [X][2,2-$(CO)_2$-2-L-*closo*-2,1-$FeCB_{10}H_{11}$] **7a** (X = $NHMe_3$, L = CO), **7b** [X = $N(PPh_3)_2$, L = PPh_3].[4] These compounds contain *closo*-2,1-MCB_{10} cage frameworks, as opposed to the more familiar *closo*-3,1,2-MC_2B_9 systems, and it was of interest to determine whether they like **1** would react with appropriate reagents to

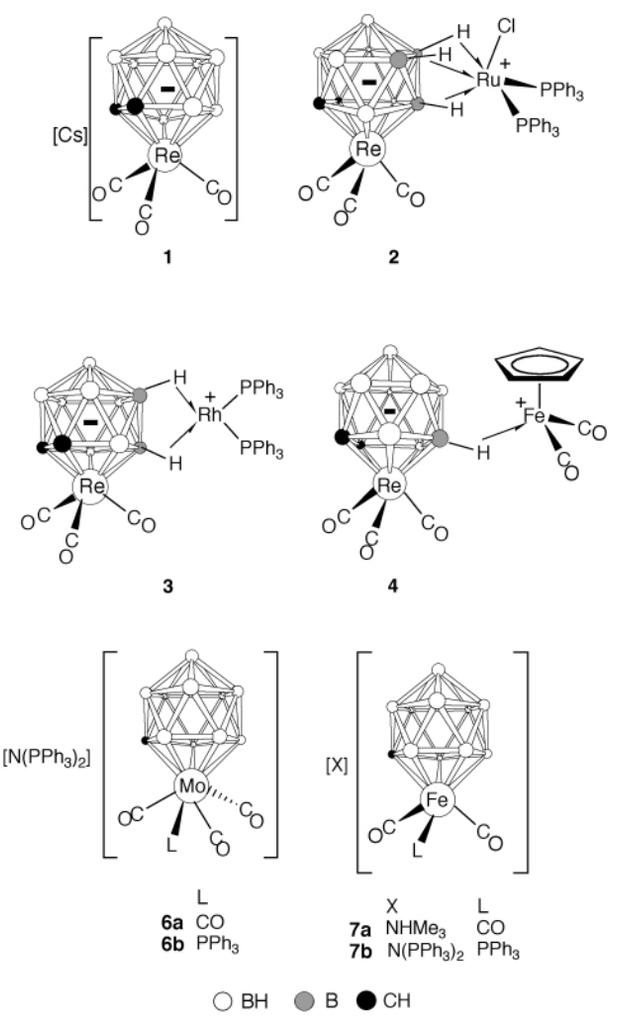

DOI: 10.1039/b003766o

give zwitterionic bimetal compounds. In this paper we report studies with **6** and **7**. Complex **6b** formed products more stable and in better yield than those obtained from **6a**, so the former was used as the preferred reagent to test the ability of a *closo*-2,1-$MoCB_{10}$ cage to ligate an exopolyhedral metal fragment. Products could be obtained using both **7a** or **7b**, depending on the exopolyhedral metal fragment employed.

Results and discussion

Compound **6b** in CH_2Cl_2 reacted with a mixture of CuCl, PPh_3 and $Tl[PF_6]$ to give the bimetal complex [2,2,2-$(CO)_3$-2-PPh_3-7,8,12-$(\mu$-H$)_3$-7,8,12-{Cu(PPh_3)}-*closo*-2,1-$MoCB_{10}H_8$] **8** isolated by column chromatography. Microanalytical, IR and NMR data for **8** are given in Tables 1–3. However, these were

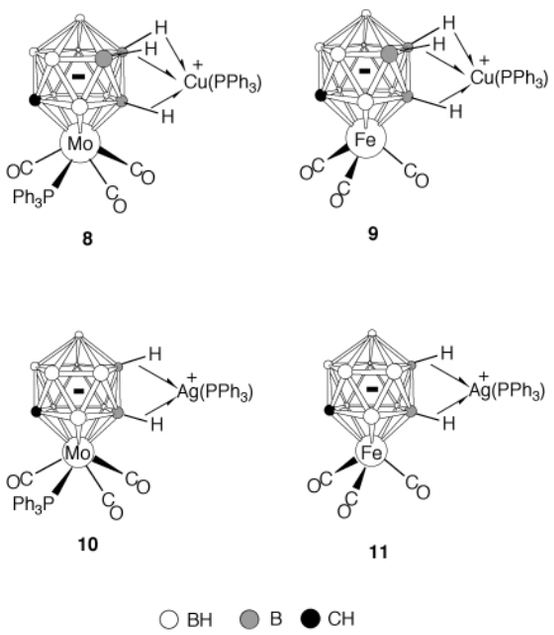

insufficient to establish the structure of the molecule because dynamic activity in solution as revealed by NMR spectroscopy masked specific structural features, such as the exact mode of attachment of the $[Cu(PPh_3)]^+$ fragment to the molybdenacarbaborane cage. A single-crystal X-ray diffraction study was therefore undertaken. Selected connectivities and angles

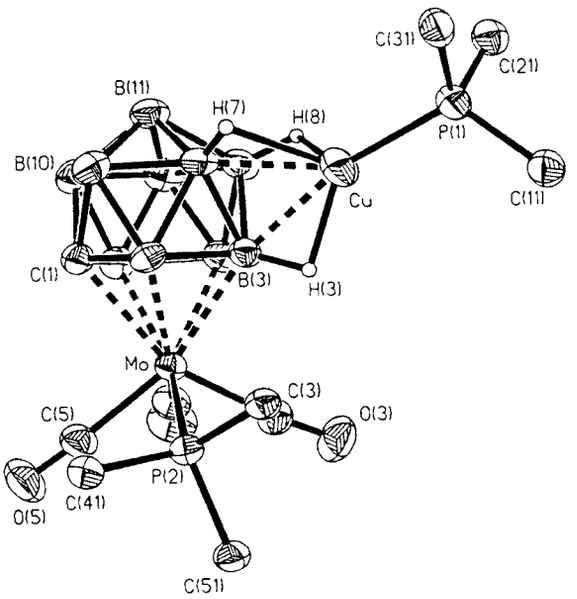

Fig. 1 Molecular structure of [2,2,2-$(CO)_3$-2-PPh_3-7,8,12-$(\mu$-H$)_3$-7,8,12-{Cu(PPh_3)}-*closo*-2,1-$MoCB_{10}H_8$] **8** showing the crystallographic labelling scheme. Hydrogen atoms, except for H(3), H(7) and H(8) are omitted for clarity, as are all but the *ipso*-carbons of the Ph rings. Thermal ellipsoids are shown at the 40% probability level (for all structures depicted).

are given in Table 4 and the molecule is shown in Fig. 1. It is immediately apparent that the $[Cu(PPh_3)]^+$ fragment is attached exopolyhedrally to the cage framework by three B–H⟶Cu three-centre two-electron bonds, one of which involves B(3), the boron vertex in a β site with respect to the carbon in the CB*B*BB ring ligating the molybdenum atom [B(3)–Cu 2.188(5) Å], while the other two involve B–H vertices in the pentagonal B_5 belt [B(7)–Cu 2.245(6) and B(8)–Cu 2.352(6) Å]. There is no direct Mo–Cu bond and the complex is thus a zwitterionic species formed by combination of the fragments [2,2,2-$(CO)_3$-2-PPh_3-*closo*-2,1-$MoCB_{10}H_{11}]^-$ and $[Cu(PPh_3)]^+$. It is interesting to compare the structure of **8** with those of [2,2-$(PEt_3)_2$-7,11-$(\mu$-H$)_2$-2,7,11-{Cu(PPh_3)}-*closo*-2,1-$PtCB_{10}H_9$][5] and [3-PPh_3-4,8-$(\mu$-H$)_2$-3,4,8-{Cu(PPh_3)}-*closo*-3,1,2-$CuC_2B_9H_9$].[6] These species have direct Pt–Cu and Cu–Cu connectivities which are bridged by two B–H⟶Cu linkages employing B–H vertices in the CBBBB and CCBBB rings coordinated to Pt and Cu,

Table 1 Analytical and physical data

Compound	Colour	Yield (%)	ν_{max}(CO)[a]/(cm^{-1})	Analysis (%)[b] C	H
8 [2,2,2-$(CO)_3$-2-PPh_3-7,8,12-$(\mu$-H$)_3$-7,8,12-{Cu(PPh_3)}-*closo*-2,1-$MoCB_{10}H_8$]	Yellow	79	2026vs, 1956s, 1925s	53.5 (53.4)	4.6 (4.6)
9 [2,2,2-$(CO)_3$-7,8,12-$(\mu$-H$)_3$-7,8,12-{Cu(PPh_3)}-*closo*-2,1-$FeCB_{10}H_8$]	Colourless	68	2082s, 2023m	44.0 (44.3)	4.4 (4.5)
10 [2.2.2-$(CO)_3$-2-PPh_3-7,12-$(\mu$-H$)_2$-7,12-{Ag(PPh_3)}-*closo*-2,1-$MoCB_{10}H_9$]	Yellow	40	2023vs, 1952s, 1921s	50.0 (50.9)	4.4 (4.4)
11 [2,2,2-$(CO)_3$-7,12-$(\mu$-H$)_2$-7,12-{Ag(PPh_3)}-*closo*-2,1-$FeCB_{10}H_9$]	Colourless	72	2076s, 2017s	41.5 (41.2)	4.1 (4.1)
12 [2,2,2-$(CO)_3$-2-PPh_3-7,8,12-$(\mu$-H$)_3$-7,8,12-{RuCl$(PPh_3)_2$}-*closo*-2,1-$MoCB_{10}H_8$]	Orange-red	71	2026vs, 1960s, 1937s	[c]53.6 (53.7)	4.7 (4.4)
13 [2,2,2-$(CO)_3$-7,8,12-$(\mu$-H$)_3$-7,8,12-{RuCl$(PPh_3)_2$}-*closo*-2,1-$FeCB_{10}H_8$]	Orange	60	2082s, 2029m	52.3 (51.6)	4.7 (4.4)
14 [2,2,2-$(CO)_3$-2-PPh_3-12-$(\mu$-H)-12-{Fe$(CO)_2(\eta$-$C_5Me_5)$}-*closo*-2,1-$MoCB_{10}H_{10}$]	Orange-red	40	2042s, 2020vs, 2002s, 1942s, 1924s	49.6 (49.8)	5.0 (5.0)
15a [2,2,2-$(CO)_3$-12-$(\mu$-H)-12-{Fe$(CO)_2(\eta$-$C_5Me_5)$}-*closo*-2,1-$FeCB_{10}H_{10}$][d]	Orange	72	2070s, 2047m, 2011s		
15b [2,2-$(CO)_2$-2-PPh_3-12-$(\mu$-H)-12-{Fe$(CO)_2(\eta$-$C_5Me_5)$}-*closo*-2,1-$FeCB_{10}H_{10}$]	Orange	76	2044m, 2005s, 1955m	53.3 (52.7)	5.9 (5.5)

[a] Measured in CH_2Cl_2; broad medium-intensity bands observed at *ca.* 2550 cm^{-1} in the spectra of all compounds are due to B–H absorptions. [b] Calculated values are given in parentheses. [c] Crystallizes with 1.0 mol equivalent CH_2Cl_2. [d] Complex **15a** is a closely related analogue of **15b**, for which adequate microanalytical data were obtained.

Table 2 Hydrogen-1 and carbon-13 NMR data[a]

Compound	^{1}H, δ[b]	^{13}C, δ[c]
8	7.34–7.52 (m, 30 H, Ph), 1.89 (s, 1 H, cage CH)	235.2 [d, CO, *J*(PC) 7], 232.2 [d, CO × 2, *J*(PC) 29], 134.0–128.8 (Ph), 57.5 (cage CH)
9	7.41–7.51 (m, 15 H, Ph), 2.03 (s, 1 H, cage CH)	206.5 (CO), 134.0–129.2 (Ph), 52.5 (cage CH)
10	7.37–7.54 (m, 30 H, Ph), 1.78 (s, 1 H, cage CH)	237.0 [d, CO, *J*(PC) 8], 233.3 [d, CO × 2, *J*(PC) 29], 134.1–128.7 (Ph), 56.8 (cage CH)
11	7.42–7.54 (m, 15 H, Ph), 1.96 (s, 1 H, cage CH)	207.2 (CO), 134.1–129.6 (Ph), 51.7 (cage CH)
12[d]	7.37–7.08 (m, 90 H, Ph), 1.73, 1.39 (s × 2, 2 H, cage CH), −3.15† [dq br, 1 H, B–H⟶Ru, *J*(PH) *ca.* 47, *J*(BH) *ca.* 104], −5.28† [dq br, 1 H, B–H⟶Ru, *J*(PH) *ca.* 50, *J*(BH) *ca.* 88], −16.20 [br, 2 H, B–H⟶Ru]	236.1 [d, CO, *J*(PC) 6], 233.1 [d, CO, *J*(PC) 7], 231.1† [d, CO, *J*(PC) 29], 230.8* [d, CO × 2, *J*(PC) 29], 229.9† [d, CO, *J*(PC) 30], 137.5–127.9 (Ph), 56.9, 52.4 (cage CH)
13[e]	7.16–7.50 (m, 30 H, Ph), 1.90,‡ 1.84 (s × 2, 2 H, cage CH), −2.83 [dq br, 1 H, B–H⟶Ru, *J*(PH) *ca.* 40, *J*(BH) *ca.* 101], −4.03 [dq br, 1 H, B–H⟶Ru, *J*(PH) *ca.* 44, *J*(BH) *ca.* 105], −15.11 [q br, 1 H, B–H⟶Ru, *J*(BH) *ca.* 78]	205.3 (CO), 205.2‡ (CO), 134.9–127.9 (Ph), 51.2,‡ 50.1 (cage CH)
14[f]	7.28–7.49 (m, 30 H, Ph), 1.97‡ (s, 1 H, cage CH), 1.93 (s, 1 H, cage CH), 1.84‡ (s, 15 H, C_5Me_5), 1.80 (s, 15 H, C_5Me_5), −18.53 [q br, 1 H, B–H⟶Fe, *J*(BH) *ca.* 72]	238.1 [d, MoCO, *J*(PC) 7], 234.5 [d, MoCO × 2, *J*(PC) 28], 211.8 (FeCO), 133.8–128.6 (Ph), 97.3,‡ 96.9 (C_5Me_5), 56.1 (cage CH), 9.7,‡ 9.6 (C_5Me_5)
15a[f]	1.93 (s, 1 H, cage CH), 1.88‡ (s, 15 H, C_5Me_5), 1.82 (s, 15 H, C_5Me_5), −18.23‡ [q br, 1 H, B–H⟶Fe, *J*(BH) *ca.* 72], −18.71 [q br, 1 H, B–H⟶Fe, *J*(BH) *ca.* 75]	211.5 (CO × 2), 207.5 (CO × 3), 97.6,‡ 97.3 (C_5Me_5), 50.7, 47.8‡ (cage CH), 10.0,‡ 9.8 (C_5Me_5)
15b[f]	7.41–7.61 (m, 15 H, Ph), 1.97‡ (s, 15 H, C_5Me_5), 1.85 (s, 15 H, C_5Me_5), 1.74 (s, 1 H, cage CH), −18.43 [q br, 1 H, B–H⟶Fe, *J*(BH) *ca.* 83]	214.5‡ [d, CO × 2, *J*(PC) 24], 214.2 [d, CO × 2, *J*(PC) 24], 213.6‡ [d, CO × 2, *J*(PC) 23], 211.9 (CO × 2), 211.8,‡ 211.7‡ (CO × 2), 134.6–128.4 (Ph), 97.3,‡ 97.1 (C_5Me_5), 49.8 (cage CH), 10.4,‡ 9.8 (C_5Me_5)

[a] Chemical shifts (δ) in ppm, coupling constants (*J*) in Hz, measurements at ambient temperatures in CD_2Cl_2. [b] Resonances for terminal BH protons occur as broad unresolved signals in the range δ *ca.* −1 to 3. [c] ^{1}H-decoupled chemical shifts are positive to high frequency of $SiMe_4$. [d] Composed of a 1 : 1 mixture of α and β isomer sets **12ab** and **12de** (see text). Peaks marked with an asterisk or a dagger are unambiguously assigned to **12ab** or **12de**, respectively. [e] Composed of a 4 : 1 mixture of isomers **13c** and **13f** (see text). Peaks marked with a double dagger are due to the minor isomer. [f] Peaks marked with a double dagger are due to a minor isomer.

Table 3 Boron-11 and phosphorus-31 NMR data[a]

Compound	^{11}B, δ[b]	^{31}P, δ[c]
8	1.8 (1 B), −10.6 (4 B), −14.1 (3 B), −16.4 (2 B)	50.9 (MoP), 9.8 (CuP)
9	9.8 (1 B), −4.9 (2 B), −8.0 (2 B), −13.6 (4 B), −17.0 (1 B)	9.16 (br, CuP)
10	1.8 (1 B), −9.4 (4 B), −12.9 (2 B), −13.9 (2 B), −14.9 (1 B)	51.5, 18.2 [d × 2, *J*(^{109}AgP) 771, *J*(^{107}AgP) 681]
11	9.5 (1 B), −5.2 (4 B), −12.5 (2 B), −13.3 (1 B), −15.0 (2 B)	17.3 [d × 2, *J*(^{109}AgP) 782, *J*(^{107}AgP) 689]
12[d]	4.7, −1.4, −8.8, −12.9, −17.1, −18.2	56.3† (br, RuP), 50.1* (vbr, RuP), 48.6 (MoP), 48.0 (MoP), 41.5† (br, RuP)
13[e]	13.6 (1 B), −5.8 (4 B), −12.5 (2 B), −13.3 (1 B), −15.0 (2 B)	55.7 [d, *J*(PP) 21], 52.7,‡ 50.4 [d, *J*(PP) 21]
14[f]	0.9 (1 B), −4.6 (2 B), −10.8 (4 B), −16.9 (3 B)	52.9,‡ 51.5
15a[f]	9.5 (1 B), −3.2 (2 B), −6.5 (2 B), −11.1 (2 B), −16.0 (2 B), −17.3[g] (1 B)	
15b[f]	5.2 (1 B), −4.6 (2 B), −6.5 (2 B), −13.5 (2 B), −17.7 (3 B)	66.0, 65.9‡

[a] Chemical shifts (δ) in ppm, coupling constants (*J*) in Hz, measurements at room temperature in CD_2Cl_2. [b] Chemical shifts (δ) are positive to high frequency of $BF_3{\cdot}Et_2O$ (external). Signals ascribed to more than one boron nucleus may result from overlapping peaks and do not necessarily indicate symmetry equivalence. [c] Hydrogen-1 decoupled, chemical shifts are positive to high frequency of 85% H_3PO_4 (external). [d] Peak integrals could not be assigned in the ^{11}B NMR spectrum because solutions of the complex consist of a mixture of α and β isomers, **12ab** and **12de** (1 : 1), and the signals are broad and overlapping. In the ^{31}P NMR spectrum, peaks marked with an asterisk or a dagger are unambiguously assigned to **12ab** or **12de**, respectively. [e] Composed of a 4 : 1 mixture of isomers **13c** and **13f** (see text). Peaks marked with a double dagger are due to the minor isomer. [f] Peaks marked with a double dagger are due to a minor isomer. [g] Identified as the B–H⟶Fe boron nucleus in the fully coupled ^{11}B NMR spectrum.

Table 4 Selected bond lengths (Å) and angles (°) for the compound [2,2,2-$(CO)_3$-2-PPh_3-7,8,12-(μ-H)$_3$-7,8,12-{Cu(PPh_3)}-*closo*-2,1-$MoCB_{10}H_8$] **8**

Mo–C(3)	1.970(5)	Mo–C(4)	1.991(5)	Mo–C(5)	2.004(5)	Mo–B(3)	2.360(5)
Mo–B(4)	2.370(5)	Mo–B(5)	2.370(5)	Mo–B(2)	2.389(5)	Mo–C(1)	2.402(4)
Mo–P(2)	2.5634(12)	C(3)–O(3)	1.142(5)	C(4)–O(4)	1.144(5)	C(5)–O(5)	1.142(5)
B(3)–Cu	2.188(5)	B(7)–Cu	2.245(6)	B(8)–Cu	2.352(6)	Cu–H(3)	1.77(4)
Cu–H(7)	2.03(4)	Cu–H(8)	2.12(4)	Cu–P(1)	2.1682(14)		
C(3)–Mo–C(4)	75.7(2)	C(3)–Mo–C(5)	114.1(2)	C(4)–Mo–C(5)	75.1(2)		
C(3)–Mo–P(2)	77.29(14)	C(4)–Mo–P(2)	129.7(2)	C(5)–Mo–P(2)	78.45(14)		
O(3)–C(3)–Mo	173.3(4)	O(4)–C(4)–Mo	179.7(5)	O(5)–C(5)–Mo	175.2(4)		
Cu–B(3)–Mo	164.3(3)	P(1)–Cu–B(3)	167.61(14)	P(1)–Cu–B(7)	143.4(2)		
B(3)–Cu–B(7)	47.6(2)	P(1)–Cu–B(8)	142.71(14)	B(3)–Cu–B(8)	46.3(2)		
B(7)–Cu–B(8)	45.3(2)						

respectively. In compound **8** the copper atom acquires a coordination of four by ligating the PPh_3 group and having three rather than two B–H⟶Cu bonds. Although H(3), H(7) and H(8) were located in the X-ray diffraction study of **8** and their positions refined, diagnostic resonances for the B–H⟶Cu groups were not observed in the ^1H and ^{11}B-{^1H} NMR spectra (Tables 2 and 3) in the expected regions δ −5.5 to −11 (^1H) and 10–30 (^{11}B-{^1H}), respectively.[7] As discussed previously the absence of these signals is likely due to exchange processes which are fast on the NMR timescale and involve rapid equilibration of the B–H⟶Cu bonds between different B–H vertices.[2,5,8] All other resonances in the NMR spectra (Tables 2 and 3) were as expected.

The combination between $[Cu(PPh_3)]^+$ and the anion of compound **7a** proceeds in a similar manner as that with **6b**, affording the zwitterionic species [2,2,2-$(CO)_3$-7,8,12-$(\mu$-H$)_3$-7,8,12-{$Cu(PPh_3)$}-*closo*-2,1-$FeCB_{10}H_8$] **9** data for which are given in Tables 1–3. Again signals due to the B–H⟶Cu groups were not observed in the ^1H and ^{11}B-{^1H} NMR spectra even at low temperatures. A broad peak is seen in the ^{31}P-{^1H} NMR spectrum at δ 9.16 as is typical for such a phosphine bound to copper,[2] and the ^1H NMR spectral integration confirms the presence of one PPh_3 ligand. Crystals of **9** proved to be poorly diffracting, nevertheless the gross features of an X-ray study revealed a molecular structure akin to that of **8**.

The salts **6b** and **7a** were next treated with [Ag(THF)-(PPh_3)][BF_4] (THF = tetrahydrofuran) which was generated *in situ* by addition of PPh_3 to Ag[BF_4] in THF. These reactions gave the complexes [2,2,2-$(CO)_3$-2-PPh_3-7,12-$(\mu$-H$)_2$-7,12-{$Ag(PPh_3)$}-*closo*-2,1-$MoCB_{10}H_9$] **10** and [2,2,2-$(CO)_3$-7,12-$(\mu$-H$)_2$-7,12-{$Ag(PPh_3)$}-*closo*-2,1-$FeCB_{10}H_9$] **11**, respectively, data for which are summarized in Tables 1–3. There were no observable diagnostic signals for the expected B–H⟶Ag groups in the ^1H or ^{11}B-{^1H} NMR spectra of **10** and **11** indicating a low energy dynamic process as with complexes **8** and **9**, and accredited to the scrambling of the $[Ag(PPh_3)]^+$ moiety about the polyhedral metallacarbaborane surface. This behaviour was previously observed for the complex [3,3,3-$(CO)_3$-3,8-{$Ag(PPh_3)$}-8-$(\mu$-H)-*closo*-3,1,2-$ReC_2B_9H_{10}$].[2] In order to ascertain a precise solid state structure and eliminate the possibility of metal–silver bond formation, an X-ray diffraction study was carried out on a single crystal of **10**. Selected bond distances and angles are listed in Table 5 and the molecule is shown in Fig. 2. The $[Ag(PPh_3)]^+$ fragment is ligated in a dihapto manner by B–H⟶Ag bonds from the cage B(3) and B(8) atoms [Ag–B(3) 2.522(4) and Ag–B(8) 2.589(4) Å]. Atoms H(3) and H(8) were located with reasonable precision from electron density maps. As with **8**, it is a cage vertex [B(3)] lying in a β site in the CB*B*BB ring coordinated to the molybdenum which forms one of the agostic bonds, the other emanating from the B–H vertex antipodal to the cage carbon. Moreover as can be seen with complex **8** the *endo*-$Mo(CO)_3(PPh_3)$ group is oriented so that the PPh_3 ligand is transoid to the *exo*-$[Ag(PPh_3)]^+$ moiety, presumably to reduce steric interactions. An unusual feature of the structure is that within the unit cell there appears to be a weak intermolecular B–H⟶Ag interaction between Ag and the B(7′)–H(7′) bond from the molecule in the adjacent asymmetric unit [Ag · · · B(7′) 3.338(4) Å]. Symmetry considerations also require the B(7)–H(7) bond to interact in an identical manner with the Ag′ atom of the neighbouring asymmetric unit as shown in Fig. 2.

Any electrophilicity of the $(B–H⟶)_2Ag(PPh_3)$ system could have been satisfied in the solid state by a third intramolecular B–H⟶Ag contact, as it is in complexes **8** and **9** for the $[Cu(PPh_3)]^+$ fragment. Certainly the silver(I) centre is capable of accommodating four ligands. Subtle differences in unit cell architecture might account in part for this disparity in behaviour for the silver and copper systems. The only submolecular dimensional variable between the intrinsic structures of **8** and **10** is the atomic radius of silver *versus* that of copper. Both **8** and **10** crystallize in the same space group ($P\bar{1}$) with similar unit cell dimensions (Table 8). A significant difference is

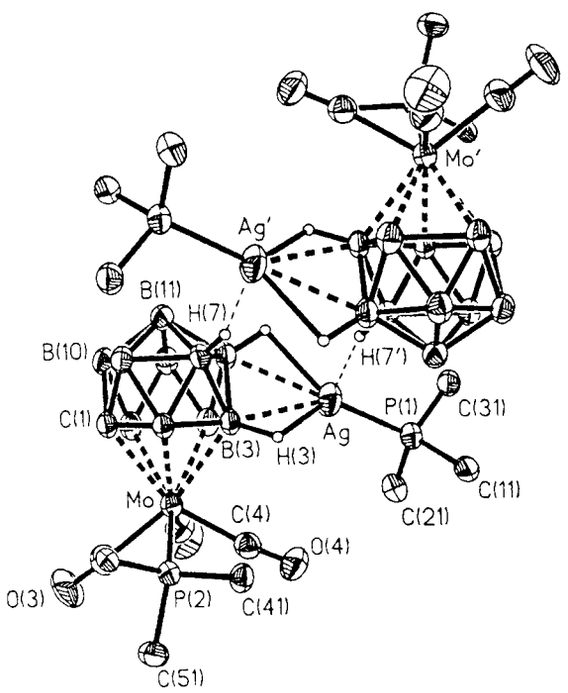

Fig. 2 Molecular structure of [2,2,2-$(CO)_3$-2-PPh_3-7,12-$(\mu$-H$)_2$-7,12-{$Ag(PPh_3)$}-*closo*-2,1-$MoCB_{10}H_9$] **10** showing the crystallographic labelling scheme. Hydrogen atoms, except for H(3), H(7) and H(8), are omitted for clarity, as are all but the *ipso*-carbons of the Ph rings.

Table 5 Selected bond lengths (Å) and angles (°) for compound [2,2,2-$(CO)_3$-2-PPh_3-7,12-$(\mu$-H$)_2$-7,12-{$Ag(PPh_3)$}-*closo*-2,1-$MoCB_{10}H_9$] **10**

Mo–C(4)	1.983(4)	Mo–C(2)	1.989(5)	Mo–C(3)	2.020(4)	Mo–B(5)	2.365(4)
Mo–B(4)	2.384(4)	Mo–B(2)	2.396(4)	Mo–C(1)	2.397(3)	Mo–B(3)	2.397(4)
Mo–P(2)	2.5774(10)	B(3)–Ag	2.522(4)	B(7)–Ag	3.540(4)	B(8)–Ag	2.589(4)
C(2)–O(2)	1.132(5)	C(3)–O(3)	1.132(5)	C(4)–O(4)	1.145(4)	Ag–H(3)	2.03(3)
Ag–H(8)	2.21(4)	Ag · · · B(7′)	3.338(4)	Ag–H(7′)	2.29(4)	Ag–H(7)	3.75(3)
Ag–P(1)	2.3724(11)						
C(4)–Mo–C(2)	76.2(2)	C(4)–Mo–C(3)	111.9(2)	C(2)–Mo–C(3)	75.1(2)		
C(4)–Mo–P(2)	76.71(11)	C(2)–Mo–P(2)	129.26(13)	C(3)–Mo–P(2)	76.53(12)		
Mo–B(3)–Ag	125.6(2)	O(2)–C(2)–Mo	179.5(5)	O(3)–C(3)–Mo	174.8(4)		
O(4)–C(4)–Mo	173.5(3)	B(7)–Ag–B(8)	28.3(10)	B(7′)–Ag–B(8)	94.1(10)		
P(1)–Ag–B(3)	147.4(10)	P(1)–Ag–B(7)	174.6(7)	P(1)–Ag–B(7′)	104.1(7)		
P(1)–Ag–B(8)	155.3(10)	B(3)–Ag–B(8)	41.1(10)	B(3)–Ag–B(7)	28.3(10)		
B(3)–Ag–B(7′)	98.0(10)						

Symmetry transformation used to generate equivalent atoms: $-x$, $-y+1$, $-z+1$.

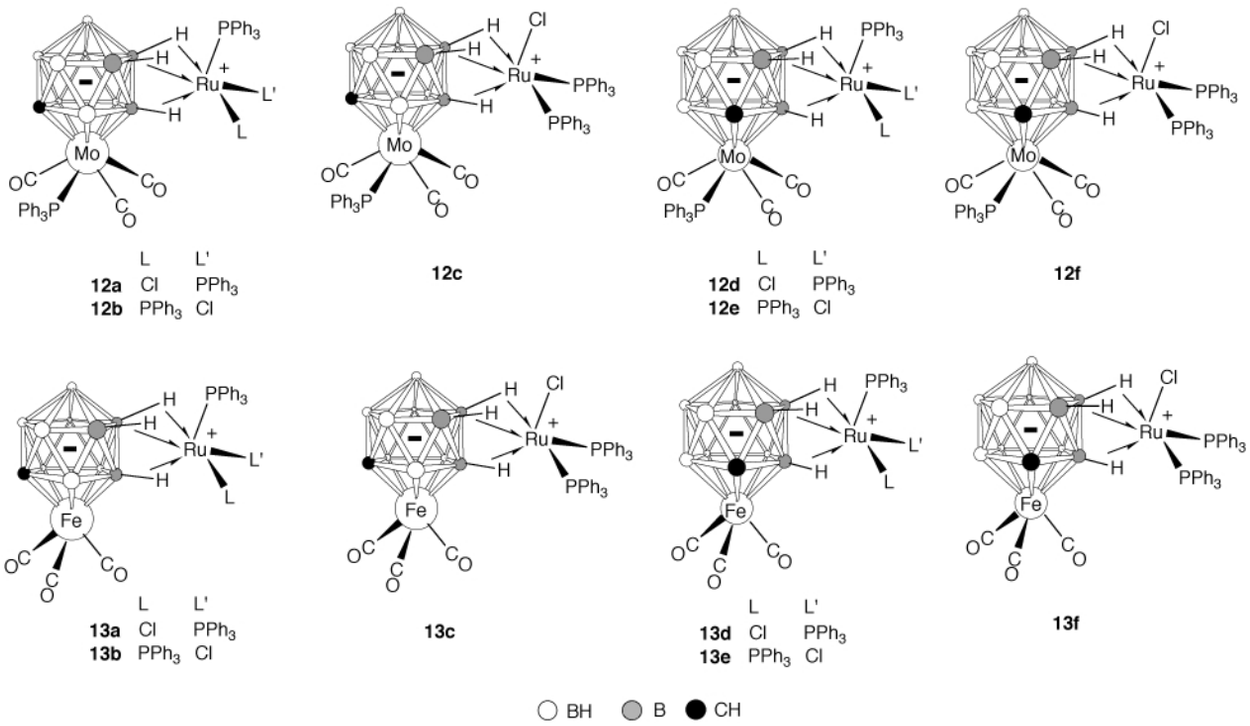

that the *b* axis in **10** is some 2.5 Å longer than that in **8** in order to accommodate the CH_2Cl_2 molecule, which occurs in the asymmetric unit of **10** but not **8**, as confirmed by analysis of packing diagrams. There is one other important difference. In the solid state structure of **8** the Cu–PPh_3 connectivity lies distinctly *anti* to the β-B(3) atom in the CB*B*BB belt [P(1)–Cu–B(3) 167.61(14)°]. In the structure of **10** the Ag–PPh_3 bond is *syn* to this boron atom [P(1)–Ag–B(3) 147.4(10)°] and *anti* to the C-antipodal B atom [P(1)–Ag–B(8) 155.3(10)°] although these angles are not vastly dissimilar. These differences are readily seen when comparing Figs. 1 and 2. Ignoring momentarily the higher electrode potentials of Ag^+ ions over Cu^+ ions, one might expect a stable or metastable copper(I) centre to be more electrophilic than Ag^I due to its smaller atomic radius. Furthermore, the availability of vacant copper(I) 4p orbitals for overlap with B–H σ bonds to form B–H⟶Cu linkages should be greater than that for vacant silver(I) 5p orbitals because of the former's lower energy. This would account for the co-ordination of three B–H bonds to the *exo*-$[Cu(PPh_3)]^+$ fragment as opposed to just two for the *exo*-$[Ag(PPh_3)]^+$ moiety. Thus the intermolecular B–H⟶Ag interactions in **10** are likely to be artefacts of optimal crystal packing, the slightly larger size of Ag^I and the disposition of the PPh_3 ligand facilitating approach of the B–H bond from the molecule in the other asymmetric unit. The B(7)–Ag′/B(7′)–Ag lengths indicate that the interaction is perhaps more electrostatic ($B–H^{\delta-} \cdots Ag^{\delta+}$) in nature rather than due to covalent bonding.

In the $^{31}P-\{^1H\}$ NMR spectrum of compound **10** (Table 3) the resonance for the $[Ag(PPh_3)]^+$ group (δ 18.2) is readily distinguishable from that for $Mo(PPh_3)$ (δ 51.5) since the former appears as a pair of concentric doublets due to $^{109}Ag–^{31}P$ and $^{107}Ag–^{31}P$ coupling.[9] The $^{31}P-\{^1H\}$ NMR spectrum of **11** displayed similar features for its $[Ag(PPh_3)]^+$ group. Low temperature NMR studies on complexes **8**–**11** did not reveal any suppression of the dynamic processes. A similar situation was reported for the complexes [3,3,3-$(CO)_3$-3,8-{$M(PPh_3)$}-8-(μ-H)-*closo*-3,1,2-$ReC_2B_9H_{10}$] (M = Cu or Ag).[2]

As mentioned earlier the salt **1** reacts with $[RuCl_2(PPh_3)_3]$ to give the *exo-closo* complex **2** with the $[RuCl(PPh_3)_2]^+$ group attached in a tridentate manner by three B–H⟶Ru bonds to the *closo*-3,1,2-ReC_2B_9 framework.[2] The X-ray diffraction study and NMR spectra of compound **2** revealed that it was formed predominantly as one isomer with C_s symmetry having a mirror plane through the Re, Ru, Cl and apical boron atoms as a result of employment of the β-B–H vertex in the agostic linkage involving the CCB*B*B ring. Analysis of a set of weak NMR signals observed for samples of **2** led to the proposal that three non-equivalent agostic B–H⟶Ru interactions are present in an asymmetrical minor isomer, one using the α-boron atom in the CC*B*BB belt and the other two from the adjacent B_5 ring. In both the major and minor species the Ru–Cl bond lies *anti* to the rhenium vertex of the *closo* rhenacarbaborane. These results prompted an investigation of the reactions between $[RuCl_2(PPh_3)_3]$ and **6b** and **7a**. The products were [2,2,2-$(CO)_3$-2-PPh_3-7,8,12-(μ-H)$_3$-7,8,12-{$RuCl(PPh_3)_2$}-*closo*-2,1-$MoCB_{10}H_8$] **12** and [2,2,2-$(CO)_3$-7,8,12-(μ-H)$_3$-7,8,12-{$RuCl(PPh_3)_2$}-*closo*-2,1-$FeCB_{10}H_8$] **13**, respectively. The NMR spectra revealed that these complexes were formed as a mixture of isomers, a feature discussed further below.

Suitable single crystals of one isomer of complex **12** were obtained for an X-ray diffraction study and selected structural parameters are listed in Table 6 and the molecule is shown in Fig. 3. The *exo*-$[RuCl(PPh_3)_2]^+$ fragment is ligated by three B–H⟶Ru bonds with B(3)–Ru 2.462(2), B(7)–Ru 2.388(2) and B(8)–Ru 2.292(2) Å.† Thus a β vertex in the CB*B*BB belt is exopolyhedrally bonded to the ruthenium atom, but in **12** it is this contact which seems to be the weaker of the three, based on bond lengths. This is in contrast with the structure of complex **2** where this agostic link was revealed to be the shortest [β-B–Ru 2.310(3) *versus* 2.379(3) and 2.462(3) Å for the other two B–Ru bonds]. This reordering of B–Ru distances in the solid state structure **12** is primarily a result of the unexpected orientation observed for the *exo*-$[RuCl(PPh_3)_2]^+$ moiety with respect to the *closo*-2,1-$MoCB_{10}$ group, *i.e.* with one of the PPh_3 ligands lying in the position *anti* to the molybdenum vertex, not the chloride ligand as in complex **2**. With the chloride exerting a weaker *trans* influence than the PPh_3 ligands, the B(8)–Ru connectivity, which lies *trans* to the chloride, is thus the shortest of the three contacts. Of the remaining two B–Ru distances, which are both

† B–Ru distances are discussed as opposed to H–Ru distances because of the lack of precision of the latter in comparison with the former from X-ray diffraction data.

Table 6 Selected bond lengths (Å) and angles (°) for compound [2,2,2-(CO)$_3$-2-PPh$_3$-7,8,12-(μ-H)$_3$-7,8,12-{RuCl(PPh$_3$)$_2$}-*closo*-2,1-MoCB$_{10}$H$_8$] **12a**

Mo–C(4)	1.992(2)	Mo–C(3)	2.013(2)	Mo–C(5)	2.028(2)	Mo–B(3)	2.326(2)
Mo–B(4)	2.381(2)	Mo–B(2)	2.393(2)	Mo–B(5)	2.404(2)	Mo–C(1)	2.419(2)
Mo–P(2)	2.5636(7)	C(3)–O(3)	1.143(2)	C(4)–O(4)	1.139(3)	C(5)–O(5)	1.136(3)
B(3)–Ru	2.462(2)	B(7)–Ru	2.388(2)	B(8)–Ru	2.292(2)	Ru–H(8)	1.73(2)
Ru–H(3)	2.00(2)	Ru–H(7)	2.01(2)	Ru–P(3)	2.2892(6)	Ru–P(1)	2.3011(7)
Ru–Cl(1)	2.3931(7)						
C(4)–Mo–C(3)	76.37(9)	C(4)–Mo–C(5)	75.15(9)	C(3)–Mo–C(5)	122.51(8)		
C(4)–Mo–P(2)	119.63(6)	C(3)–Mo–P(2)	76.32(6)	C(5)–Mo–P(2)	76.20(6)		
B(3)–Mo–P(2)	144.58(5)	O(3)–C(3)–Mo	176.8(2)	O(4)–C(4)–Mo	177.8(2)		
O(5)–C(5)–Mo	175.3(2)	Mo–B(3)–Ru	169.59(10)	P(3)–Ru–B(8)	111.77(6)		
P(3)–Ru–P(1)	97.59(3)	B(8)–Ru–P(1)	107.70(5)	P(3)–Ru–B(7)	149.49(5)		
B(8)–Ru–B(7)	43.22(7)	P(1)–Ru–B(7)	106.53(5)	P(3)–Ru–Cl(1)	94.61(2)		
B(8)–Ru–Cl(1)	141.88(6)	P(1)–Ru–Cl(1)	94.88(3)	B(7)–Ru–Cl(1)	101.53(6)		
P(3)–Ru–B(3)	108.11(5)	B(8)–Ru–B(3)	43.13(7)	P(1)–Ru–B(3)	146.62(5)		
B(7)–Ru–B(3)	42.99(7)	Cl(1)–Ru–B(3)	103.67(5)				

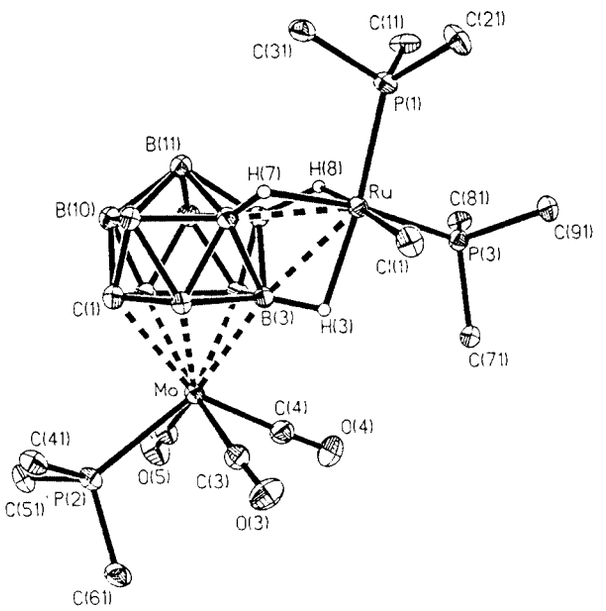

Fig. 3 Molecular structure of [2,2,2-(CO)$_3$-2-PPh$_3$-7,8,12-(μ-H)$_3$-7,8,12-{RuCl(PPh$_3$)$_2$}-*closo*-2,1-MoCB$_{10}$H$_8$] **12a** showing the crystallographic labelling scheme. Hydrogen atoms, except for H(3), H(7) and H(8) are omitted for clarity, as are all but the *ipso*-carbons of the Ph rings.

trans to PPh$_3$ ligands, β-B(3)–Ru is longer because of likely steric repulsion between the *endo*-Mo(CO)$_3$(PPh$_3$) and *exo*-[RuCl(PPh$_3$)$_2$]$^+$ fragments, a feature discussed further below. Therefore the molecule observed in the crystal structure adopts the conformation **12a**, along with its enantiomeric partner **12a′** (Scheme 1), as is required for a centrosymmetric space group. This is one of six possible diastereomeric pairs of enantiomers, **12a**–**12f**, all of which are asymmetric and are expected accordingly to give rise to complicated NMR spectra, where discrimination between isomers is a difficult task. Indeed the NMR spectra recorded at ambient temperatures (see below) indicate the presence of at least two sets of isomers in solution. The Mo(CO)$_3$(PPh$_3$) vertex adopts a four-legged piano stool arrangement with the Mo(PPh$_3$) group positioned transoid to the β-B(3)H(3) vertex [P(2)–Mo–B(3) 144.58(5)°], presumably to minimize steric impact with the *exo*-[RuCl(PPh$_3$)$_2$]$^+$ group. This is also believed to be the cause of the unexpected orientation of the latter moiety in the crystal structure. For this reason it is not unreasonable to eliminate isomers **12c** and **12f** from our discussion of the complex structure in solution and we will focus on two sets of isomers, designated as the β set (**12aa′bb′**) and the α set (**12dd′ee′**) (Scheme 1). A similar orientational isomerism involving *exo*-[RuCl(PPh$_3$)$_2$]$^+$ groups was reported recently for the complexes [10,10′-Hg(5,6,10-(μ-H)$_3$-5,6,10-{RuCl(PPh$_3$)$_2$}-*nido*-7,8-C$_2$B$_9$H$_8$)$_2$] and [5,6,10-(μ-H)$_3$-5,6,10-{RuCl(PPh$_3$)$_2$}-*endo*-10-(9′-Hg-*closo*-1′,2′-C$_2$B$_{10}$H$_{11}$)-*nido*-7,8-C$_2$B$_9$H$_8$].[10]

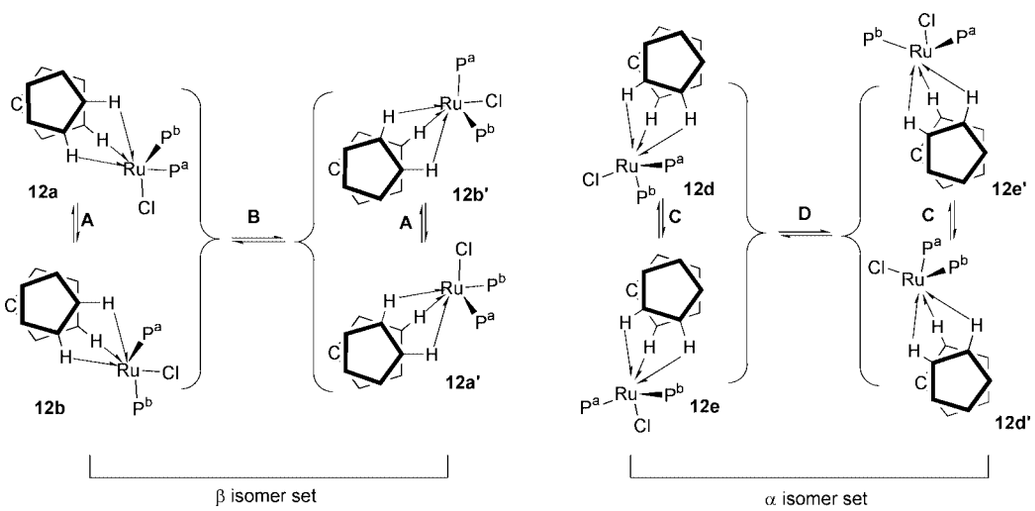

Scheme 1 Dynamic processes for complex **12**. Diastereomeric exchange A and C = rotational twisting of the *exo*-[RuCl(PPh$_3$)$_2$]$^+$ fragment. Enantiomeric exchange B and D = translational scrambling of the *exo*-[RuCl(PPh$_3$)$_2$]$^+$ fragment. Only the antiprismatic CBBB B and B$_5$ pentagonal rings of the molybdenacarbaborane are shown.

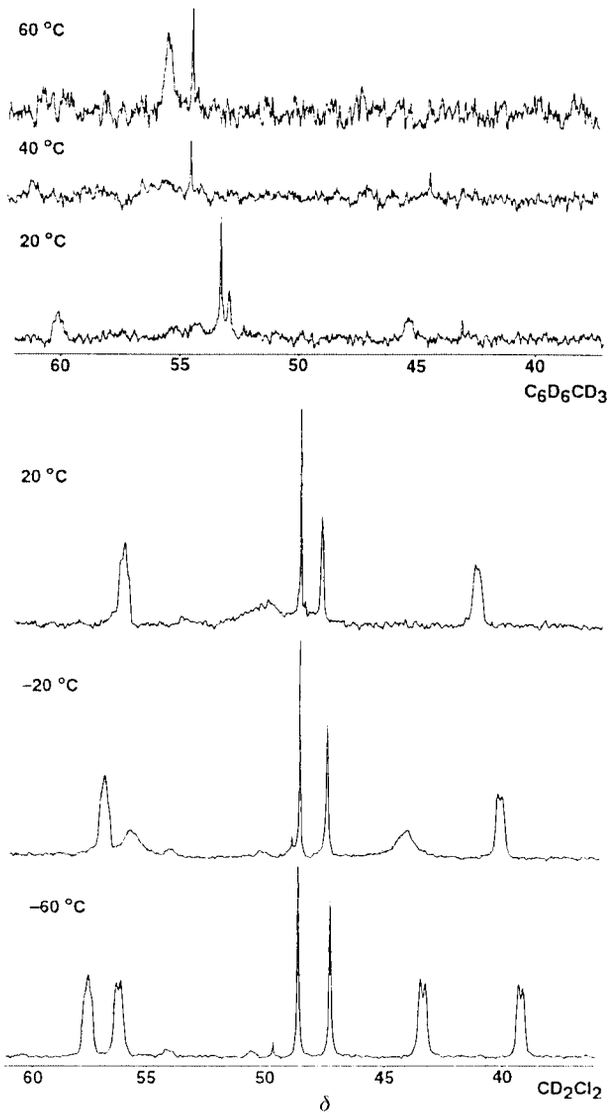

Fig. 4 Variable temperature ^{31}P-{^1H} NMR spectra for complex **12**.

The ^{11}B-{^1H} NMR spectrum of complex **12** consisted of very broad overlapping peaks, where even integral assignment was impossible, and thus this spectrum was alas completely uninformative. The ^{31}P-{^1H} NMR spectrum (Table 3 and Fig. 4) measured at room temperature displayed two sharp signals at δ 48.6 and 48.0 in a ratio of 1:1 due to $Mo(PPh_3)$ ligands in two different environments. It is postulated at this point that each signal corresponds to the isomeric α and β sets **12aa′bb′** and **12dd′ee′**, respectively. Owing to the observed ratio, the exact assignment could not confidently be made under these conditions. Also seen in this spectrum are two broad $Ru(PPh_3)_2$ signals at δ 56.3 and 41.5. These are attributed to the α set **12dd′ee′**. The signals are not as complicated as might be thought because **12d** and **12e** (and **12d′** with **12e′**) are rotamers, which we believe are interconverting by rapid rotational twisting of the *exo*-$[RuCl(PPh_3)_2]^+$ group, such that the chloride ligand exchanges between the sites *syn* to the molybdenum vertex (processes C, Scheme 1). The two $Ru(PPh_3)_2$ ligands remain diastereotopic by virtue of their difficulty in undergoing translational scrambling around the *closo*-2,1-$MoCB_{10}H_{11}$ system, *i.e.* process D in Scheme 1 is very slow on the NMR timescale. This can be understood by realizing that one α-B–H vertex is displaced from the other by a carbon vertex on one side, and two boron vertices on the other, thus introducing a significant impediment to enantiomeric interconversion. Almost unnoticed in this room temperature ^{31}P-{^1H} NMR spectrum was a very broad peak centred at δ 50.1 ($\nu_{1/2}$ = *ca.* 300 Hz). Low temperature ^{31}P-{^1H} NMR spectra (Fig. 4), down to −60 °C, showed that this peak decoalesced into two broad doublets [δ 56.3 and 43.5, J(PP) 20 Hz]. The other peaks remained for the most part unaffected. It is suggested that, as discussed above for the α set of isomers, the β isomer set is undergoing rapid exchange between diastereoisomers (**12a** ⇌ **12b** and **12a′** ⇌ **12b′**, processes A, Scheme 1) through rotational twisting of the *exo*-$[RuCl(PPh_3)_2]^+$ group. However, the translational transformations (**12ab** ⇌ **12a′b′**, process B, Scheme 1) are also occurring at or near the ^{31}P NMR timescale at ambient temperatures. At −60 °C this process is suppressed to a kinetic level well below that of this timescale allowing differentiation between the diastereotopic PPh_3 environments. The increased facility of this exchange in the β system might be attributed to the proximity of two β-B–H vertices to each other. The *exo*-$[RuCl(PPh_3)_2]^+$ fragment can remain anchored to the B–H bond antipodal to the cage carbon atom while it flips from one β-B–H bond and the mutually adjacent B–H bond in the B_5 ring to the other pair of corresponding B–H bonds which lie the other side of a plane encompassing the Re, Mo, Cl and apical B atoms. Such a process, if occurring fast enough, will transform this plane into a pseudo mirror symmetry element, thus rendering the $Ru(PPh_3)_2$ ligands in the β set of isomers chemically equivalent.

Thus it became imperative to measure high temperature NMR spectra for complex **12**. The most suitable solvent for this purpose was d_8-toluene, though it was found that the room temperature ^{31}P-{^1H} NMR spectrum using this solvent contained a different proportion of α and β isomer sets (1:2) than in CD_2Cl_2 (1:1) (Fig. 4). Thus in d_8-toluene the α set of isomers (**12dd′ee′**) gives rise to broad peaks at δ 56.5 and 41.3 due to the inequivalent $Ru(PPh_3)_2$ ligands and a sharp signal at δ 48.2 for the $Mo(PPh_3)$ ligand. A very broad signal ($\nu_{1/2}$ = *ca.* 300 Hz) at δ *ca.* 50.1 results from the $Ru(PPh_3)_2$ ligands of the predominant β set (**12aa′bb′**), whose constituent enantiomers are at or near a state of coalescence. Also seen is a sharp signal (δ 49.1) for the $Mo(PPh_3)$ ligand in this set. The solvent dependency of the α:β ratio confirms that the α ⇌ β interconversion process is occurring in solution but is very slow on the general NMR timescale, with the relative rates for intra-set enantiomeric exchange remaining about the same judging by the peak linewidths observed for both solvents. At 40 °C in d_8-toluene no discernible peaks could be identified in the ^{31}P-{^1H} NMR spectrum. At 60 °C one broad signal [δ 54.2, $Ru(PPh_3)_2$] and one sharp signal [δ 53.3, $Mo(PPh_3)$] were observed. Thus, at this elevated temperature, it appears that there is more or less unfettered interconversion between all isomers of both α and β sets at rates faster than the NMR timescale.

The room temperature ^1H NMR spectrum of complex **12** displayed two peaks for the cage CH protons for each of the isomer sets (δ 1.39 and 1.73) in a 1:1 ratio in CD_2Cl_2. Also observed was a high field broad quartet at δ −16.20 integrating to two protons. Unfortunately no ^{11}B–^1H coupling could be resolved, primarily because it is believed to result from the overlap of two broad quartets, one from each isomer set. This should be compared with the highest field signal observed in the same spectrum of complex **2** [δ −14.84, J(BH) *ca.* 80 Hz]. As discussed elsewhere,[2,7] the lineshape and coupling are diagnostic for a B–H⟞M proton, but the chemical shift was unusually low, with such agostic systems normally expected to resonate in the region δ −5 to −11.[7] Two other resonances are seen in the ^1H NMR spectrum of complex **12** at δ −3.15 and −5.28, each with ^{11}B–^1H couplings [J(BH) *ca.* 104 and *ca.* 88 Hz, respectively] and with apparent ^{31}P–^1H doublet couplings [J(PH) *ca.* 47 and *ca.* 50 Hz, respectively]. The integration for both these peaks is for one proton each only. The following explanation might account for the number and integration of these signals. Since the α set of isomers is likely to be limited to

the rotational diastereomeric exchange already described, all three B–H⟶Ru protons are observed (δ −3.15, −5.28 and −16.20). The β set is more dynamic at room temperature and only one B–H⟶Ru proton can be observed, and this is tentatively suggested as being the anchor agostic linkage referred to above, *i.e.* at the boron vertex antipodal to the cage carbon atom. This resonance overlaps with that observed at δ −16.20 for the α isomers, hence the integration to two protons. It is still unclear why one of the agostic protons for any one isomer set should resonate so far downfield. For complex **2** it was proposed that this was an indicator for the presence of a β-B–H⟶M bond (from the CCB*B*B coordinating ring) in the absence of direct metal–metal bonding. It is interesting that a B–H⟶M bridge from the B_5 belt in complex **12** might also be responsible for such a high field resonance. A ^{1}H NMR spectrum at −60 °C displayed three very broad peaks at δ *ca.* −3.2, −5.4 and −16.2 with a 2:2:2 integration but with no pertinent coupling information. A doublet at δ 230.8 in the ^{13}C-{^{1}H} NMR spectrum of **12** with *J*(PC) 29 Hz is ascribed to equivalent mutually transoid $Mo(CO)_2$ carbonyl ligands of the β set of isomers (**12aa′bb′**). A single doublet is detected because the dynamic process D discussed above must be occurring faster on the ^{13}C NMR timescale, so that these CO ligands are rendered chemically equivalent. The same carbonyls in the α set (**12dd′ee′**) are, as expected, inequivalent displaying two resonances at δ 231.1 [*J*(PC) 29] and 229.9 [*J*(PC) 30 Hz].

Tractable crystals of complex **13** could not be procured for the purpose of an unambiguous structure identification. However, it is immediately apparent that this complex does not suffer the same steric congestion seen in compound **12**. Thus we believe that isomers **13c** and **13f** (and their enantiomeric partners), where the chloride ligand lies *anti* to the iron vertex, are the only important contributors to the NMR spectra. Complex **13** in fact consists of a 4:1 mixture of isomers based on integrals measured in the NMR spectra. The ^{31}P-{^{1}H} NMR spectrum displays two doublets at δ 55.7 and 50.4 [*J*(PP) 21 Hz] due to the inequivalent PPh_3 ligands in the major isomer. Despite their mutual *syn* positions with respect to the molybdenum vertex, there can still be no mirror plane when a vertex in the CBBBB belt is utilized in B–H⟶Ru bonding. A peak at δ 52.7 was all that could be identified for the minor isomer, a second peak probably being obscured by one of the larger signals. The ^{11}B-{^{1}H} and ^{11}B NMR spectra were once again unhelpful because of the high degree of overlapping of broad signals. The ^{1}H NMR spectrum was more useful with three B–H⟶Ru resonances observed at δ −2.83, −4.03 and −15.11, with ^{11}B–^{1}H couplings of 101, 105 and 78 Hz, respectively. The first two of these also showed ^{31}P–^{1}H coupling constants of *ca.* 40 and 44 Hz, and are likely due to the B–H⟶Ru linkages employing the B_5 ring vertices, these lying *trans* to each of the phosphine ligands as shown. This implies that the B–H⟶Ru group, formed from the CBBBB belt, is responsible for the high field resonance at δ −15.11, in contrast with complex **12**. If the **13c** ⟹ **13f** interconversion is occurring it takes place very slowly. Since both the isomers are formally asymmetric, confidently determining which of these is the major species is not possible. However, reactions with complex **5** have shown that a β-B–H bond is invariably used for bridging Re–M bonds in dimetal complexes[3] and this observation persuades us that **13c** is likely to be the major isomer.

As previously reported[2] the salt **1** reacted with $[Fe(CO)_2(THF)(\eta\text{-}C_5H_5)][BF_4]$ to yield the zwitterionic complex **4**. In a variation of this reaction, treatment of **1** with $[Fe(CO)_2(THF)(\eta\text{-}C_5Me_5)][BF_4]$ yielded an inseparable 1:1 mixture of two isomeric species [3,3,3-$(CO)_3$-*n*-(μ-H)-*n*-{$Fe(CO)_2(\eta\text{-}C_5Me_5)$}-*closo*-3,1,2-$ReC_2B_9H_{10}$] (*n* = 7 or 8). One isomer had a structure similar to that of **4**. In solution this molecule is symmetrical since a mirror plane can be generated by free rotation about the B–H⟶Fe system. This symmetry is a consequence of the β-boron of the CCB*B*B ring being involved in the agostic bridge. The second isomer most likely has an unsymmetrical structure with one of the two α-borons in the CC*B*BB ring forming the B–H⟶Fe bond, as indicated from NMR studies.[2] These results made it of interest to establish whether $[Fe(CO)_2(THF)(\eta\text{-}C_5R_5)][BF_4]$ (R = H or Me) would react with **6b** or **7a** to afford bimetallic species. It was quickly established that treatment of **6b** with $[Fe(CO)_2(THF)(\eta\text{-}C_5H_5)][BF_4]$ afforded a product that was unstable, so attention focused on $[Fe(CO)_2(THF)(\eta\text{-}C_5Me_5)][BF_4]$. The reagent $[Fe(CO)_2(THF)(\eta\text{-}C_5Me_5)][BF_4]$ was generated *in situ* in THF from $[FeI(CO)_2(\eta\text{-}C_5Me_5)]$ and $Ag[BF_4]$. After removal of solvent, addition of **6b** and CH_2Cl_2 gave the stable complex [2,2,2-$(CO)_3$-2-PPh_3-12-(μ-H)-12-{$Fe(CO)_2(\eta\text{-}C_5Me_5)$}-*closo*-2,1-$MoCB_{10}H_{10}$] **14**. Both complexes **7a** and **7b** reacted with $[Fe(CO)_2(THF)(\eta\text{-}C_5Me_5)][BF_4]$ to yield the compounds [2,2-$(CO)_2$-2-L-12-(μ-H)-12-{$Fe(CO)_2(\eta\text{-}C_5Me_5)$}-*closo*-2,1-$FeCB_{10}H_{10}$] **15a** (L = CO), **15b** (L = PPh_3). Analytical and spectroscopic data for these three complexes are given in Tables 1–3.

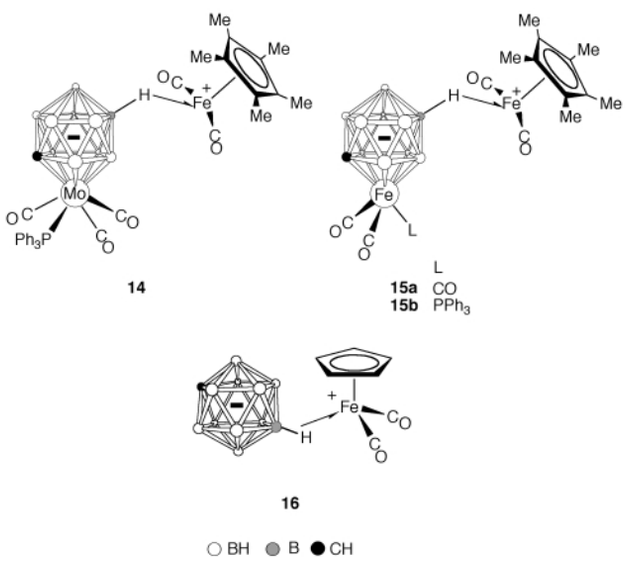

In order to place the molecular structures of the zwitterionic molecules **14** and **15** on a firm basis a single-crystal X-ray diffraction study was carried out on **14**. Selected structural parameters are given in Table 7 and the molecule is shown in Fig. 5. The cationic $[Fe(CO)_2(\eta\text{-}C_5Me_5)]^+$ and anionic [2,2,2-$(CO)_3$-2-PPh_3-*closo*-2,1-$MoCB_{10}H_{11}]^-$ fragments are held together by a single agostic B–H⟶Fe bridge at B(8), a boron atom situated in the pentagonal B_5 belt above the molybdenum ligating CBBBB ring and antipodal to the cage carbon atom. This is in distinct contrast with the structure of **4** where the B–H⟶Fe system involves the β-boron atom in the CCB*B*B rhenium-coordinating ring. There is current interest in employing weakly coordinating anions to stabilize highly reactive cations and among the anions studied for this purpose has been [*closo*-$CB_{10}H_{11}]^-$.[11] As part of a general study the zwitterionic species **16** was characterized by Reed and co-workers.[12] The electronic relationship between the groups BH and $Mo(CO)_3(PPh_3)$ or $Fe(CO)_2(L)$ (L = CO or PPh_3), each providing an electron pair for cluster bonding, results in a striking correlation between the structures of the molecules **14**, **15a** and **15b** with **16**. The *endo* metal–ligand groups in the first three are notionally replaced by a B–H vertex in the last. In **16** the bridging H atom was located from the X-ray data with an Fe–H distance of 1.563(2) Å. The H(8) atom in **14** was unfortunately not located with any precision but was inserted in a calculated

Table 7 Selected internuclear distances (Å) and angles (°) for [2,2,2-$(CO)_3$-2-PPh_3-12-(μ-H)-12-{$Fe(CO)_2(\eta\text{-}C_5Me_5)$}-*closo*-2,1-$MoCB_{10}H_{10}$] **14**

Mo–C(4)	1.952(12)	Mo–C(5)	2.008(9)	Mo–C(3)	2.019(9)	Mo–B(2)	2.362(11)
Mo–B(4)	2.363(10)	Mo–B(3)	2.367(11)	Mo–B(5)	2.399(9)	Mo–C(1)	2.408(9)
Mo–P	2.538(3)	C(3)–O(3)	1.132(9)	C(4)–O(4)	1.153(12)	C(5)–O(5)	1.138(9)
Fe–H(8)	1.5556	Fe–B(8)	2.622(11)	Fe–C(8)	1.762(14)	Fe–C(9)	1.81(2)
Fe–C(7)	1.87(2)	Fe–C(10)	1.87(2)	Fe–C(40)	2.038(11)	Fe–C(44)	2.041(13)
Fe–C(41)	2.061(11)	Fe–C(43)	2.098(12)	Fe–C(42)	2.105(10)	C(7)–O(7)	1.17(2)
C(8)–O(8)	1.14(2)	C(9)–O(9)	1.15(2)	C(10)–O(10)	1.20(2)		
C(4)–Mo–C(5)	74.0(5)	C(4)–Mo–C(3)	76.1(5)	C(5)–Mo–C(3)	122.5(4)		
C(4)–Mo–B(2)	124.3(4)	C(5)–Mo–B(2)	155.8(4)	C(3)–Mo–B(2)	80.0(4)		
C(4)–Mo–B(4)	80.4(4)	C(5)–Mo–B(4)	94.5(4)	C(3)–Mo–B(4)	127.1(4)		
C(4)–Mo–B(3)	83.3(4)	C(5)–Mo–B(3)	137.4(4)	C(3)–Mo–B(3)	84.7(4)		
C(4)–Mo–B(5)	118.8(4)	C(5)–Mo–B(5)	83.9(3)	C(3)–Mo–B(5)	153.4(3)		
C(4)–Mo–C(1)	151.9(4)	C(5)–Mo–C(1)	114.8(4)	C(3)–Mo–C(1)	114.7(4)		
C(4)–Mo–P	122.4(3)	C(5)–Mo–P	78.3(4)	C(3)–Mo–P	78.0(3)		
B(2)–Mo–P	100.0(3)	B(4)–Mo–P	151.7(3)	B(3)–Mo–P	143.4(3)		
B(5)–Mo–P	106.9(2)	C(1)–Mo–P	85.6(2)	O(3)–C(3)–Mo	173.2(9)		
O(4)–C(4)–Mo	176.0(9)	O(5)–C(5)–Mo	173.0(12)	C(11)–P–Mo	116.3(4)		
C(21)–P–Mo	112.0(3)	C(31)–P–Mo	116.9(3)	B(8)–H(8)–Fe	161.3		
H(8)–Fe–C(8)	97.2	H(8)–Fe–C(9)	90.1	H(8)–Fe–C(7)	86.5		
C(8)–Fe–C(7)	90.3(10)	H(8)–Fe–C(10)	81.5	C(9)–Fe–C(10)	88(2)		
C(7)–Fe–C(10)	131(2)	O(7)–C(7)–Fe	177(2)	O(8)–C(8)–Fe	159(2)		
O(9)–C(9)–Fe	141(4)	O(10)–C(10)–Fe	171(4)				

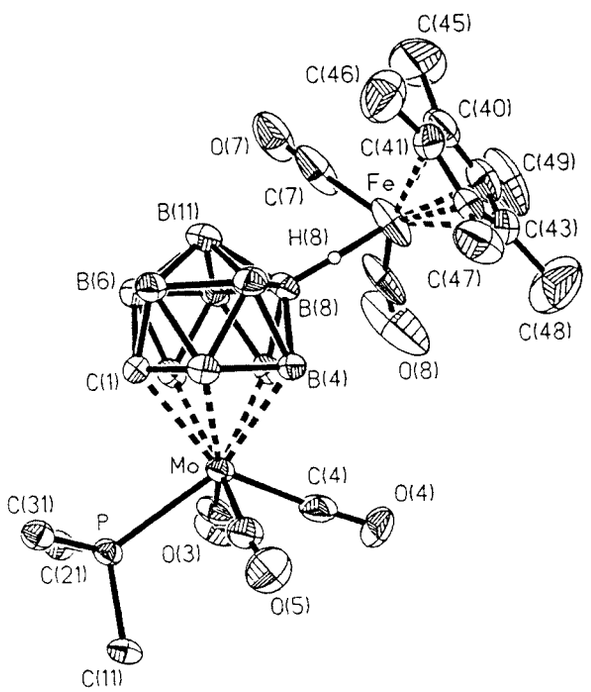

Fig. 5 Molecular structure of [2,2,2-$(CO)_3$-2-PPh_3-12-(μ-H)-12-{$Fe(CO)_2(\eta\text{-}C_5Me_5)$}-*closo*-2,1-$MoCB_{10}H_{10}$] **14** showing the crystallographic labelling scheme. Hydrogen atoms, except for H(8) are omitted for clarity, as are all but the *ipso*-carbons of the Ph rings.

position [Fe–H(8) 1.556 Å]. The Fe–B(8) distance [2.622(11) Å] in **14**, however, compares well with that found [2.593(2) Å] in **16**.[12]

It has been determined that for the monocarbon carbaborane anion [*closo*-$CB_{10}H_{11}]^-$ the B–H vertex antipodal to the carbon is the most electron rich site of the molecule, thus rationalizing the location of the *exo*-[$Fe(CO)_2(\eta\text{-}C_5H_5)]^+$ fragment in the structure of compound **16**.[11,12] For metallacarbaboranes there clearly will be some accumulation of extra electron density at sites adjacent to the metal. Indeed for 1,2-R_2-*closo*-3,1,2-$MC_2B_9H_9$ (R = H or Me) systems activation of vertices not in the coordinating $\overline{CCBBB}$ ring is quite rare.[2,13] In the complexes **6b** and **7b**, B–H vertices in both pentagonal rings can clearly function as donors to an electrophilic metal centre. It seems plausible that with bulky ligands such as PPh_3 and $\eta\text{-}C_5Me_5$ in complex **14** on the molybdenum and iron atoms, respectively, the $\overline{CBBBB}$ sites in the molybdenacarbaborane fragment are not as readily accessible. Thus while the B–H vertex antipodal to the cage carbon may or may not be the most electronically favourable site for *exo*-ML_n binding, it would at the very least be the next best option and should be sterically more feasible anyway.

In solution, NMR resonances for complex **14** are readily identified. This molecule gives rise to a high field broad quartet in the ^{1}H NMR spectrum at δ −18.53 [*J*(BH) *ca.* 72 Hz]. This may be compared with the corresponding signal (δ −18.46) for the isomers of the complex related to **4** mentioned above where an *exo*-[$Fe(CO)_2(\eta\text{-}C_5Me_5)]^+$ fragment is attached to either the α or β sites in the $\overline{CCBBB}$ ring in a 1 : 1 mixture. This appears as a broad irresolute peak due to the overlap of the B–H⟞Fe resonances of both the α and β isomers.[2] In the ^{13}C-{^{1}H} NMR spectrum of **14** two doublet resonances (δ 238.1 and 234.5) were observed for the $Mo(CO)_3$ carbonyl carbons in a ratio of 1 : 2, with typical *transoid* and *cisoid* ^{31}P–^{13}C coupling constants of 7 and 28 Hz, respectively. This is possible providing there is free rotation about the B–H⟞Fe system and so the molecule will possess pseudo C_s symmetry on the NMR timescale. It would not be possible if any one vertex in the coordinating $\overline{CBBBB}$ belt were utilized, confirming that the solid state structure is, for the most part, retained in solution. All other NMR spectral details are in accordance with this formulation, with the exception of several peaks due to a minor species. This is most evident from the ^{31}P-{^{1}H} NMR spectrum which shows resonances at δ 51.5 due to the major component and a smaller peak at δ 52.9 for the minor. The latter also produces observable peaks in the ^{1}H NMR spectrum at δ 1.97 (cage CH) and 1.84 (C_5Me_5) as well as in the ^{13}C-{^{1}H} NMR spectrum at δ 97.3 (C_5Me_5) and 9.7 ($C_5\mathit{Me}_5$). The ratio of these isomers estimated from the NMR spectra is 3 : 1.

For both complexes **15a** and **15b** there are also major and minor species present in solution, both with the same ratio of 3 : 1. For example the ^{31}P-{^{1}H} NMR spectrum of complex **15b** revealed singlet peaks for the major (δ 66.0) and minor (δ 65.9) species. A broad quartet is seen in the ^{1}H NMR spectrum of complex **15a** at δ −18.71 [*J*(BH) *ca.* 75 Hz] for the B–H⟞Fe group in the major species, which partially obscures the corresponding weaker signal for the minor isomer [δ −18.23, *J*(BH) *ca.* 72 Hz]. For complex **15b** this spectrum displays a broad quartet for the major isomer at δ −18.43 [*J*(BH) *ca.* 83 Hz] with no observable counterpart for the minor isomer,

probably because it is completely obscured. The ^{13}C-{^{1}H} NMR spectrum of **15b** is more helpful with a singlet resonance for the carbaborane-FeCO carbonyl carbons [δ 214.2, J(PC) 24 Hz] and a singlet resonance for the cyclopentadienyl-FeCO carbonyl carbons (δ 211.9) of the major species. The carbonyl-carbon data for **15a** are even simpler with just two resonances observed [δ 211.5 (CO × 2) and 207.5 (CO × 3)] for the *exo*- and *endo*-iron fragments, respectively. These spectral features imply pseudo mirror symmetry existing in solution for both major isomers, thus making them analogous to the salient isomer characterized for compound **14** by X-ray. Of the complexes **14** and **15** only in the ^{11}B-{^{1}H} NMR spectrum of **15a** the resonance (δ −17.3) due to the B–H⟞Fe boron nucleus could be positively identified, and even then a ^{11}B–^{1}H coupling constant could not be evaluated from the fully coupled ^{11}B NMR spectrum due to complete overlap of one of the doublet peaks. This chemical shift is, however, comparable with that observed for complex **4** [δ −22.9, J(BH) 82 Hz] in that it is at considerably higher field than normally expected for B–H⟞M groups.[7] Little can be garnered from the ^{13}C-{^{1}H} NMR spectrum for the minor isomer of compound **15a** with regard to specific structural pointers. The minor isomer of **15b** notably gives rise to signals in this spectrum with two doublet resonances for the carbaborane-FeCO carbonyl carbons and two for those of the cyclopentadienyl-FeCO carbonyl-carbon nuclei (Table 3). These signals are ascribed to a species where generation of a pseudo mirror plane is not possible in solution without breaking the B–H⟞Fe bond. It is conjecture but in the absence of more detailed information we propose that the minor isomers of complexes **14** and **15** are those with the *exo*-$[Fe(CO)_2(\eta\text{-}C_5Me_5)]^+$ groups bound to the B–H bonds in the coordinating $\overline{CBBBB}$ cage face, probably the β-B–H bond based on patterns of reactivity so far observed.

Conclusion

The metallacarbaborane anions derived from the salts **6b** and **7** have been shown to behave as tri- and bi-dentate ligands towards *exo*-$[Cu(PPh_3)]^+$ and *exo*-$[Ag(PPh_3)]^+$ groups, respectively, by utilization of B–H bonds from both the $\overline{CBBBB}$ and B_5 pentagonal rings of the cage. A tridentate bonding mode of these anions has also been identified in the complexes **12** and **13**. It is interesting that the carbaborane cage can occupy three coordination sites simultaneously on both the endo- and exo-polyhedral metal–ligand fragments, the former by penta-hapto coordination of the $\overline{CBBBB}$ face (*cf.* cyclopentadienide ligands), and the latter by the three mutually adjacent carbaborane B–H bonds. With the syntheses of the complexes **14** and **15**, the chemistry of the anions **6b** and **7** would seem to mirror that of the anion of salt **1**. However, the formation of all the new species confirms that activation of B–H bonds in the non-coordinating B_5 belt of the metallacarbaboranes *closo*-2,1-MCB_{10}, in particular the B–H vertex antipodal to the cage carbon atom, is fundamental to their reactivity towards *exo*-metal–ligand fragments. This is at variance with the behaviour of the complexes **6** and **7** towards hydride abstracting reagents, where a hydride is almost always removed from a β-B site in the $\overline{CB\textit{B}BB}$ ring and replaced by a charge-compensating neutral donor molecule such as THF.[4] This may be because the binding of an *exo*-ML_n fragment is more sterically controlled.

Experimental

General

Solvents were distilled from appropriate drying agents under nitrogen prior to use. Light petroleum refers to that fraction of boiling point 40–60 °C. All reactions were carried out under an atmosphere of dry nitrogen using Schlenk line techniques. Chromatography columns (*ca.* 15 cm in length and 2 cm in diameter) were packed with silica gel (Acros, 70–230 mesh) or alumina (Aldrich, *ca.* 150 mesh). Celite pads for filtration were *ca.* 3 cm thick. Chemicals were purchased commercially from Aldrich Chemical Co. or Acros, except $[N(PPh_3)_2][2,2,2\text{-}(CO)_3\text{-}2\text{-}PPh_3\text{-}closo\text{-}2,1\text{-}MoCB_{10}H_{11}]$ **6b** and $[X][2,2\text{-}(CO)_2\text{-}2\text{-}L\text{-}closo\text{-}2,1\text{-}FeCB_{10}H_{11}]$ **7a** (X = $NHMe_3$, L = CO), **7b** [X = $N(PPh_3)_2$, L = PPh_3] which were prepared by the methods previously described.[4] The NMR spectra reported in Tables 2 and 3 were recorded at the following frequencies: ^{1}H at 360.13, ^{13}C at 90.56, ^{31}P at 145.78 and ^{11}B at 115.5 MHz.

Preparations

$[2,2,2\text{-}(CO)_3\text{-}2\text{-}PPh_3\text{-}7,8,12\text{-}(\mu\text{-}H)_3\text{-}7,8,12\text{-}\{Cu(PPh_3)\}\text{-}closo\text{-}2,1\text{-}MoCB_{10}H_8]$ 8. The compounds **6b** (0.250 g, 0.23 mmol), CuCl (0.025 g, 0.25 mmol), PPh_3 (0.065 g, 0.25 mmol), and $Tl[PF_6]$ (0.086 g, 0.25 mmol) were treated with CH_2Cl_2 (15 cm^3) and the mixture stirred for 4 h, over which time a white precipitate formed. The suspension was filtered through Celite, and solvent then removed *in vacuo*. The residue was taken up in CH_2Cl_2 (1 cm^3) and chromatographed, eluting with CH_2Cl_2–light petroleum (2:1). The yellow fraction was collected and this gave $[2,2,2\text{-}(CO)_3\text{-}2\text{-}PPh_3\text{-}7,8,12\text{-}(\mu\text{-}H)_3\text{-}7,8,12\text{-}\{Cu(PPh_3)\}\text{-}closo\text{-}2,1\text{-}MoCB_{10}H_8]$ **8** (0.160 g) after removal of solvent.

$[2,2,2\text{-}(CO)_3\text{-}7,8,12\text{-}(\mu\text{-}H)_3\text{-}7,8,12\text{-}\{Cu(PPh_3)\}\text{-}closo\text{-}2,1\text{-}FeCB_{10}H_8]$ 9. The compounds $[Fe_3(CO)_{12}]$ (0.250 g, 0.50 mmol) and $[NHMe_3][nido\text{-}7\text{-}CB_{10}H_{13}]$ (0.100 g, 0.50 mmol) were heated at reflux in THF (10 cm^3) for 24 h to generate the salt **7a** *in situ*. The mixture was then cooled to room temperature, and CuCl (0.050 g, 0.50 mmol), PPh_3 (0.131 g, 0.50 mmol) and $Tl[PF_6]$ (0.180 g, 0.50 mmol) were added. After stirring for 24 h at ambient temperatures solvent was removed *in vacuo* and the residue treated with CH_2Cl_2 (20 cm^3). Following filtration through a Celite plug, *ca.* 2 g of silica gel were added to the filtrate. Solvent was removed *in vacuo* affording a yellow brownish powder which was transferred to the top of a chromatography column. Elution with CH_2Cl_2–light petroleum (4:1) gave a yellow fraction. Removal of solvent *in vacuo* followed by crystallization from CH_2Cl_2–light petroleum yielded pale yellow microcrystals of $[2,2,2\text{-}(CO)_3\text{-}7,8,12\text{-}(\mu\text{-}H)_3\text{-}7,8,12\text{-}\{Cu(PPh_3)\}\text{-}closo\text{-}2,1\text{-}FeCB_{10}H_8]$ **9** (0.203 g).

$[2,2,2\text{-}(CO)_3\text{-}2\text{-}PPh_3\text{-}7,12\text{-}(\mu\text{-}H)_2\text{-}7,12\text{-}\{Ag(PPh_3)\}\text{-}closo\text{-}2,1\text{-}MoCB_{10}H_9]$ 10. The compounds $Ag[BF_4]$ (0.040 g, 0.20 mmol) and PPh_3 (0.052 g, 0.20 mmol) were treated with THF (10 cm^3) and the mixture stirred for 20 min to generate *in situ* a solution of $[Ag(PPh_3)(THF)][BF_4]$. This was transferred to a pressure-equalized dropping funnel and added over 15 min to a second Schlenk tube containing compound **6b** (0.200 g, 0.18 mmol) dissolved in THF (10 cm^3) and cooled to −78 °C. The funnel was then replaced by a stopper and the mixture, which became cloudy, was gradually warmed to room temperature and stirred for 2 h. The suspension was filtered through Celite, and the solvent then removed *in vacuo*. The residue was taken up in CH_2Cl_2 (1 cm^3) and chromatographed, eluting with CH_2Cl_2–light petroleum (2:1). A yellow fraction was collected which gave $[2,2,2\text{-}(CO)_3\text{-}2\text{-}PPh_3\text{-}7,12\text{-}(\mu\text{-}H)_2\text{-}7,12\text{-}\{Ag(PPh_3)\}\text{-}closo\text{-}2,1\text{-}MoCB_{10}H_9]$ **10** (0.106 g) after removal of solvent *in vacuo*.

$[2,2,2\text{-}(CO)_3\text{-}7,12\text{-}(\mu\text{-}H)_2\text{-}7,12\text{-}\{Ag(PPh_3)\}\text{-}closo\text{-}2,1\text{-}FeCB_{10}H_9]$ 11. The compounds $[Fe_3(CO)_{12}]$ (0.250 g, 0.50 mmol) and $[NHMe_3][nido\text{-}7\text{-}CB_{10}H_{13}]$ (0.100 g, 0.50 mmol) were heated in THF (10 cm^3) at reflux for 24 h to generate the reagent **7a**. The mixture was then cooled to room temperature, and a solution of PPh_3 (0.130 g, 0.50 mmol) and $Ag[BF_4]$ (0.100 g, 0.50 mmol) in THF (10 cm^3) was added. After stirring for 24 h at ambient temperature, the solvent was removed *in vacuo* and the residue treated with CH_2Cl_2 (20 cm^3). Following filtration through

Table 8 Data for crystal structure analysis of compounds **8**, **10**, **12a** and **14**

	8	**10**	**12a**	**14**
Chemical formula	$C_{40}H_{41}B_{10}CuMoO_3P_2$	$C_{41}H_{43}AgB_{10}Cl_2MoO_3P_2$	$C_{64}H_{70}B_{10}Cl_3MoO_3P_3Ru$	$C_{34}H_{41}B_{10}FeMoO_5P$
M	899.25	1028.50	1391.57	820.53
Crystal system	Triclinic	Triclinic	Triclinic	Orthorhombic
Space group	$P\bar{1}$	$P\bar{1}$	$P\bar{1}$	$Pna2_1$
a/Å	11.7020(12)	11.146(2)	11.1520(18)	20.0653(15)
b/Å	12.1224(8)	14.6174(12)	13.811(3)	16.9217(17)
c/Å	16.203(2)	16.121(4)	21.962(4)	11.7368(15)
α/°	92.074(9)	70.670(11)	105.442(9)	
β/°	104.602(10)	84.02(2)	95.010(14)	
γ/°	106.685(7)	69.706(10)	93.19(2)	
U/Å^3	2115.9(4)	2324.6(7)	3237.0(11)	3985.1(7)
Z	2	2	2	4
μ(Mo-Kα)/cm^{-1}	9.12	9.12	6.70	7.57
T/K	293	293	173	293
Reflections measured	7835	8622	33811	3901
Independent reflections	7435	8161	14646	3676
R(int)	0.0274	0.0140	0.0216	0.0264
$wR2$ (all data), $R1$ [a]	0.0994, 0.0508	0.0976, 0.0379	0.0710, 0.0253	0.1035, 0.0488 [b]

[a] $F_o > 4\sigma(F_o)$. [b] Flack parameter = −0.01(5).

a Celite plug, *ca.* 2 g of silica gel were added to the filtrate. Solvent was removed *in vacuo* affording a yellow brownish powder which was transferred to the top of a chromatography column. Elution with CH_2Cl_2–light petroleum (4:1) gave a yellow fraction. Removal of solvent *in vacuo* yielded pale yellow powder of [2,2,2-$(CO)_3$-7,12-(μ-H)$_2$-7,12-{Ag(PPh_3)}-*closo*-2,1-$FeCB_{10}H_9$] **11** (0.231 g).

[2,2,2-$(CO)_3$-2-PPh_3-7,8,12-(μ-H)$_3$-7,8,12-{$RuCl(PPh_3)_2$}-*closo*-2,1-$MoCB_{10}H_8$] 12. The compounds **6b** (0.126 g, 0.11 mmol), [$RuCl_2(PPh_3)_3$] (0.120 g, 0.12 mmol), and Tl[PF_6] (0.050 g, 0.12 mmol) were dissolved in CH_2Cl_2 (15 cm^3) and the mixture was stirred for 1 h, during which time a white precipitate formed. The suspension was filtered through Celite, and the solvent removed *in vacuo*. The residue was taken up in CH_2Cl_2 (1 cm^3) and chromatographed, eluting with CH_2Cl_2–light petroleum (3:1). A very broad red-orange band was eluted which gave [2,2,2-$(CO)_3$-2-PPh_3-7,8,12-(μ-H)$_3$-7,8,12-{RuCl(PPh_3)$_2$}-*closo*-2,1-$MoCB_{10}H_8$] **12** (0.100 g) after removal of solvent *in vacuo*.

[2,2,2-$(CO)_3$-7,8,12-(μ-H)$_3$-7,8,12-{$RuCl(PPh_3)_2$}-*closo*-2,1-$FeCB_{10}H_8$] 13. The salt **7a** was prepared as above from [$Fe_3(CO)_{12}$] (0.250 g, 0.50 mmol) and [$NHMe_3$][*nido*-7-$CB_{10}H_{13}$] (0.100 g, 0.50 mmol) in THF (10 cm^3). After cooling to room temperature, [$RuCl_2(PPh_3)_3$] (0.480 g, 0.50 mmol) and Tl[PF_6] (0.180 g, 0.50 mmol) were added and the mixture was stirred for 24 h. Solvent was removed *in vacuo*, CH_2Cl_2 (20 cm^3) added to the residue, and the suspension filtered through a Celite plug. Silica gel (*ca.* 2 g) was added to the filtrate and solvent removed *in vacuo* affording an orange brownish powder. The latter was transferred to the top of a chromatography column. Elution with CH_2Cl_2–light petroleum (4:1) gave an orange fraction. Removal of solvent *in vacuo* followed by crystallization from benzene–light petroleum yielded orange microcrystals of [2,2,2-$(CO)_3$-7,8,12-(μ-H)$_3$-7,8,12-{$RuCl(PPh_3)_2$}-*closo*-2,1-$FeCB_{10}H_8$] **13** (0.280 g).

[2,2,2-$(CO)_3$-2-PPh_3-12-(μ-H)-12-{$Fe(CO)_2(\eta$-$C_5Me_5)$}-*closo*-2,1-$MoCB_{10}H_{10}$] 14. The complex [$FeI(CO)_2(\eta^5$-$C_5Me_5)$] (0.093 g, 0.25 mmol) was dissolved in THF (10 cm^3), treated with Ag[BF_4] (0.048 g, 0.25 mmol) and the mixture stirred for 30 min. The suspension was filtered through Celite, and solvent then removed *in vacuo*. Compound **6b** (0.250 g, 0.23 mmol) was added to this residue, followed by CH_2Cl_2 (15 cm^3) and the reaction mixture stirred for 2 h. Solvent was removed *in vacuo* and the residue taken up in CH_2Cl_2 (1 cm^3) and chromatographed, eluting with CH_2Cl_2–light petroleum (3:2). An orange-red fraction was collected which afforded [2,2,2-$(CO)_3$-2-PPh_3-12-(μ-H)-12-{$Fe(CO)_2(\eta$-$C_5Me_5)$}-*closo*-2,1-$MoCB_{10}H_{10}$] **14** (0.070 g) after removal of solvent *in vacuo*.

[2,2-$(CO)_2$-2-L-12-(μ-H)-12-{$Fe(CO)_2(\eta$-$C_5Me_5)$}-*closo*-2,1-$FeCB_{10}H_{10}$] 15a (L = CO), 15b (L = PPh_3). (i) A mixture of [$FeI(CO)_2(\eta$-$C_5Me_5)$] (0.190 g, 0.50 mmol) and Ag[BF_4] (0.100 g, 0.50 mmol) in THF (10 cm^3) was stirred for 30 min at room temperature and filtered through a Celite plug into a solution of the salt **7a** (0.170 g, 0.50 mmol) dissolved in THF (10 cm^3). The mixture was further stirred for 24 h at ambient temperature. Solvent was then removed *in vacuo*, and the residue treated with CH_2Cl_2 (20 cm^3). After filtration through a Celite plug, *ca.* 2 g of silica gel were added to the filtrate. Solvent was removed *in vacuo* affording an orange powder which was transferred to the top of a chromatography column. Elution with CH_2Cl_2–light petroleum (4:1) gave an orange fraction. Removal of solvent *in vacuo* followed by crystallization from benzene–light petroleum yielded orange microcrystals of [2,2,2-$(CO)_3$-12-(μ-H)-12-{$Fe(CO)_2(\eta$-$C_5Me_5)$}-*closo*-2,1-$FeCB_{10}H_{10}$] **15a** (0.373 g).

(ii) Using a similar procedure [$FeI(CO)_2(\eta$-$C_5Me_5)$] (0.190 g, 0.50 mmol), Ag[BF_4] (0.100 g, 0.50 mmol) and compound **7b** (0.520 g, 0.50 mmol) gave [2,2-$(CO)_2$-2-PPh_3-12-(μ-H)-12-{$Fe(CO)_2(\eta$-$C_5Me_5)$}-*closo*-2,1-$FeCB_{10}H_{10}$] **15b** (0.286 g).

Crystallography

Experimental data for compounds **8**, **10**, **12a** and **14** are given in Table 8. Diffracted intensities for **8**, **10** and **14** were collected on an Enraf-Nonius CAD-4 diffractometer using graphite-monochromated Mo-Kα X-radiation operating in ω (**8**) and ω–2θ (**10**, **14**) scan modes. Low-temperature data for **12a** were collected on a Siemens SMART CCD area-detector three-circle diffractometer. For four settings of φ, narrow data 'frames' were collected for 0.3° increments in ω. A total of 2132 frames of data were collected affording a sphere of data.

The structures were solved by direct methods and successive Fourier difference syntheses used to locate all non-hydrogen atoms with SHELXTL version 5.03.[14] Refinements were made by full-matrix least squares on all F^2 data using SHELXL 97.[15] Anisotropic thermal parameters were included for all non-hydrogen atoms. With the exception of the agostic B–H⋯M (M = Cu, Ag or Ru) protons in **8**, **10**, **12a** and H(7) in **10**, all hydrogen atoms were included in calculated positions and

allowed to ride on their parent boron or carbon atoms with fixed isotropic thermal parameters ($U_{iso} = 1.2U_{iso}$ of the parent atom or $U_{iso} = 1.5U_{iso}$ for the methyl protons). The agostic protons in **8**, **10**, **12a** and H(7) in **10** were located in Fourier difference syntheses. The positional parameters of these hydrogens were allowed to refine while their isotropic thermal parameters were constrained to $1.2U_{iso}$ of the parent boron atoms. Compound **10** co-crystallized with a molecule of CH_2Cl_2. The carbon atom C(90) of the solvent molecule was disordered over two sites (60:40) and, in addition, the C–Cl bond distances were restrained. Both solvent molecules of **12a** were disordered over two positions: the CH_2Cl_2 molecule (50:50), and the C_5H_{12} molecule (75:25), and individual distances, C–Cl of the CH_2Cl_2 and C–C of the pentane molecule, were restrained. The carbon atoms of the minor component of the pentane molecule were refined with isotropic thermal parameters and no hydrogen atoms added. The carbonyl groups on the iron centre of **14** [C(7), O(7), C(8), O(8), C(9), O(9), C(10), O(10)] were disordered over two sites in the ratio 70:30. The thermal parameters for the minor disordered components were refined isotropically with the value for C(9) fixed at 10.15. All calculations were carried out on Dell or Viglen PC computers.

CCDC reference number 186/2033.

See http://www.rsc.org/suppdata/dt/b0/b003766o/ for crystallographic files in .cif format.

Acknowledgements

We thank the Robert A. Welch Foundation for support (Grant AA-1201).

References

1 P. A. Jelliss and F. G. A. Stone, *J. Organomet. Chem.*, 1995, **500**, 307 and references cited therein.
2 D. D. Ellis, P. A. Jelliss and F. G. A. Stone, *Organometallics*, 1999, **18**, 4982.
3 I. Blandford, J. C. Jeffery, P. A. Jelliss and F. G. A. Stone, *Organometallics*, 1998, **17**, 1402; J. C. Jeffery, P. A. Jelliss, L. H. Rees and F. G. A. Stone, *Organometallics*, 1998, **17**, 2258.
4 D. D. Ellis, A. Franken, P. A. Jelliss, F. G. A. Stone and P.-Y. Yu, *Organometallics*, 2000, **19**, 1993.
5 S. A. Batten, J. C. Jeffery, P. L. Jones, D. F. Mullica, M. D. Rudd, E. L. Sappenfield, F. G. A. Stone and A. Wolf, *Inorg. Chem.*, 1997, **36**, 2570.
6 H. C. Kang, Y. Do, C. B. Knobler and M. F. Hawthorne, *Inorg. Chem.*, 1988, **27**, 1716.
7 S. A. Brew and F. G. A. Stone, *Adv. Organomet. Chem.*, 1993, **35**, 135.
8 J.-L. Cabioch, S. J. Dossett, I. J. Hart, M. U. Pilotti and F. G. A. Stone, *J. Chem. Soc.*, *Dalton Trans.*, 1991, 519.
9 E. L. Muetterties and C. W. Aleggranti, *J. Am. Chem. Soc.*, 1972, **94**, 6386.
10 I. A. Lobanova, V. I. Bregadze, S. V. Timofeev, P. V. Petrovskii, Z. A. Starikova and F. M. Dolgushhin, *J. Organomet. Chem.*, 2000, **597**, 48.
11 C. A. Reed, *Acc. Chem. Res.*, 1998, **31**, 133.
12 D. J. Liston, Y. J. Lee, W. R. Scheidt and C. A. Reed, *Inorg. Chem.*, 1987, **26**, 2739.
13 J. A. Long, T. B. Marder, P. E. Behnken and M. F. Hawthorne, *J. Am. Chem. Soc.*, 1984, **106**, 2979; I. T. Chizhevsky, I. A. Lobanova, V. I. Bregadze, P. V. Petrovskii, V. A. Antonovich, A. V. Polyakov, A. I. Yanovskii and Y. T. Struchkov, *Mendeleev Commun.*, 1991, 48; J. C. Jeffery, P. A. Jelliss and F. G. A. Stone, *J. Chem. Soc.*, *Dalton Trans.*, 1993, 1073.
14 SHELXTL, version 5.03, Bruker AXS, Madison, WI, 1995.
15 G. M. Sheldrick, University of Göttingen, 1997.